1987

NASA Technical Memorandum 100815

Unsteady Heat Transfer in Turbine Blade Ducts: Focus on Combustor Sources

(NASA-TM-100815) UNSTEADY HEAT TRANSFER IN TURBINE BLADE DUCTS: FOCUS ON COMBUSTOR SOURCES (NASA) 18 p CSCL 20D

N88-18870

Unclas
G3/34 0128857

Kenneth J. Baumeister
Lewis Research Center
Cleveland, Ohio

and

Ronald Huff
Huff and Associates
Cleveland, Ohio

Prepared for the
National Heat Transfer Conference
sponsored by the American Society of Mechanical Engineers
Houston, Texas, July 24–27, 1988

NASA

UNSTEADY HEAT TRANSFER IN TURBINE BLADE DUCTS: FOCUS ON COMBUSTOR SOURCES

Kenneth J. Baumeister
National Aeronautics and Space Administration
Lewis Research Center
Cleveland, Ohio 44135

and

Ronald Huff
Huff and Associates
Cleveland, Ohio

ABSTRACT

Thermal waves generated by either turbine rotor blades cutting through nonuniform combustor temperature fields or unsteady burning could lead to thermal fatigue cracking in the blades. To determine the magnitude of the thermal oscillation in blades with complex shapes and material compositions, a finite element Galerkin formulation has been developed to study combustor generated thermal wave propagation in a model two-dimensional duct with a uniform plug flow profile. The reflection and transmission of the thermal waves at the entrance and exit boundaries are determined by coupling the finite element solutions at the entrance and exit to the eigenfunctions of an infinitely long adiabatic duct. Example solutions are presented for a variety of cases. In general, thermal wave propagation from an air passage into a metallic blade wall is small and not a problem. However, if a thermal barrier coating is applied to a metallic surface under conditions of high heat transfer, a good impedance match is obtained and a significant portion of the thermal wave can pass into the blade material.

NOMENCLATURE

A	property tensor, see Eq. (5)
A^+_n	amplitude of + going n entrance mode
A^-_n	amplitude of - going n entrance mode
A_n	damping coefficient, Eq. (A7)
B^+_n	amplitude of + going exit mode
B	uniform entrance and exit duct height
c	specific heat of solid and gaseous medium at constant pressure
β_n	propagation constant, Eq. (A8)
f	frequency
h	heat transfer coefficient
Imag	imaginary part
i	$\sqrt{-1}$
k	thermal conductivity of the medium
N_m	number of modes in expansion, Eq. (6) and (A6)
n	mode number
n	unit outward normal
n^*	modified mode number, Eq. (A9)
R_e	real part
t	time
U	plug flow velocity
X	separation variable, Eq. (A3)
x	axial distance coordinate
Y	separation variable, Eq. (A3)
y	transverse distance coordinate
α	thermal diffusivity, Eq. (A2)
β	propagation constant, Eq. (B2)
Γ	thermal transfer coefficient, Eq. (11)
δ	element thickness at the wall
η	thermal impedance, Eq. (B9)
θ	spatial (transformed) temperature
θ_a	entrance dimensionless temperature
θ_b	exit dimensionless temperature, Eq. (7)

θ_t total dimensionless temperature, Eq. (2)

λ separation constant, Eq. (A4)

ρ density of propagation medium

ω angular velocity

Superscript

~ approximate finite element prediction

Subscripts

1 region 1

2 region 2

a entrance duct

b exit duct

i nodal point

i incident wave

r reflected wave

t transmitted wave

x x direction component

y y direction component

INTRODUCTION

In new aircraft combustor designs, higher outlet temperatures are being considered which could give rise to large amplitude thermal stresses in aircraft turbine blades and lead, perhaps, to thermal structure failure. Also, current earth to orbit rocket engines utilize hydrogen/oxygen gas generators that drive turbines used to power the oxygen and fuel pumps. These systems are similar to the hot section in aircraft turbine engines and therefore may experience similar dynamic thermal stresses.

In the present paper, the sources of unsteady thermal waves in the exhaust gases of a gas turbine engine will be discussed as well as how thermal waves propagate and couple to solid boundaries. Next, a finite element analysis is developed which is capable of evaluating thermal wave absorption in a duct with uniform (plug) flow and a wall composed of thermally absorbing materials.

THERMAL WAVE SOURCES

At least two mechanisms can produce thermal wave propagation in gas turbine passages. First, because of nonuniform burning in the combustor, spatial circumferential variations in the hot gas temperature field exist (Norgren and Riddlebaugh, 1985), as shown in Fig. 1. When the rotating turbine blades cut through the nonuniform circumferential temperature field, temporal harmonic thermal oscillations will be produced. For a typical turbofan engine, disturbance frequencies of 600 Hz or higher can be expected.

Secondly, large temporal variations in the temperature field can exist at a fixed spatial location resulting from unsteady burning of the air-fuel mixture (Sofrin and Riloff, 1976), as shown in Fig. 2. This temperal oscillation will effect both the turbine stator and rotor blades.

The present paper is concerned with how these thermal waves propagate and interact with the blade material.

GEOMETRIC MODEL

The curved turbine blades are modeled by the simple rectangular geometry shown in Fig. 3(a). Next, the idealized flow duct shown in Fig. 3(b) is used to simulate the flow in a turbine passage. The interior passage of the duct is assumed to be air moving with a uniform (plug) velocity profile. A metallic or ceramic blade represents the upper duct wall in the central region and the lower wall is assumed to be a line of symmetry. Outside this range the entire duct is assumed to be insulated. The stagnation region near the blade leading edge and the curvature of the passage have not been considered.

METHOD OF ANALYSIS

The thermal sources discussed in the previous section are assumed to generate a harmonic temperature field which will propagate down the duct at approximately the flow velocity (see Appendix A, Eq. (A13)). As the input driving boundary condition to this problem, a positive going thermal wave of known magnitude is assumed at the entrance ($x = 0$) of the duct. The thermal wave may be plane or may have significant transverse temperature variations. The present paper will focus on the interaction (absorption) of these "propagating" thermal duct waves with the wall blade material. High wall absorption could lead to large thermal stresses which could shorten the blade life by increasing thermal fatigue.

In the uniform infinitely long entrance and exit regions with perfectly insulated walls, the exact solution of the governing differential equation can easily be solved (see Appendix A). In contrast, exact analytical solutions are generally not possible in the central region adjacent to the turbine blade; consequently, the finite element analysis is used to determine the temperature fields both in the air passage and in the blade.

Thermal wave reflection (usually very small) at the inlet and transmission (usually large) at the duct exit are determined by matching the finite element solutions in the interior of the central region to the known analytical eigenfunction expansions in the uniform inlet and outlet ducts.

GOVERNING EQUATION

The propagation of thermal disturbances will be governed by the convective energy equation which for uniform (plug) flow, neglecting viscous dissipation, can be written as (Bird et al., 1960, Table 10.2-3)

$$\rho c \left[\frac{\partial \theta_T}{\partial t} + U\frac{\partial \theta_T}{\partial x}\right] = \frac{\partial}{\partial x}\left(k_x \frac{\partial \theta_T}{\partial x}\right) + \frac{\partial}{\partial y}\left(k_y \frac{\partial \theta_T}{\partial y}\right) \quad (1)$$

For harmonic disturbances of the form

$$\theta_T(x,y,t) = R_e \left\{ \theta(x,y) e^{i\omega t} \right\} \qquad (2)$$

Eq. (1) reduces to

$$\frac{\partial}{\partial x}\left(k_x \frac{\partial \theta}{\partial x}\right) + \frac{\partial}{\partial y}\left(k_y \frac{\partial \theta}{\partial y}\right) - \rho U c \frac{\partial \theta}{\partial x} - i\rho c\omega\theta = 0 \qquad (3)$$

For use in the finite element analysis to follow, it is convenient to express Eq. (3) in vector form

$$\nabla \cdot \left\{ \bar{\bar{A}} \cdot \nabla\theta \right\} - \rho U c \frac{\partial \theta}{\partial x} - i\omega\rho c\theta = 0 \qquad (4)$$

where the property tensor $\bar{\bar{A}}$ is represented by

$$\bar{\bar{A}} = \begin{Bmatrix} k_x & 0 \\ 0 & k_y \end{Bmatrix} \qquad (5)$$

The vector product of the tensor $\bar{\bar{A}}$ and a vector follow the common definition (Bird et al., 1960, p. 730, Eqs. (A.4) to (19)).

UNIFORM DUCT ANALYTICAL SOLUTION

The proper termination boundary condition of the finite element region requires that thermal waves are not artificially reflected by the difference equations employed at the boundary nodal points (Baumeister, 1986). The analytical solution of Eq. (3) for thermal wave propagation in a uniform insulated duct infinite in length will be employed to give the termination boundary condition for the finite element region. The analytical solution is derived in Appendix A, Eq. (A6) and will not be repeated here.

Without flow, thermal waves are highly damped in air (see discussion in Appendix A, Eq. (A10)). However, when flow is present, the thermal waves can propagate nearly undamped in the duct like their counterparts in acoustics and electromagnetics. Figure 4 shows how only a very small Mach number is required to yield a unity attenuation coefficient. Thus, the positive going wave at the entrance can be approximated as

$$\theta_a(x,y) = \sum_{n=1}^{N_m} A_n^+ \cos\left(\frac{(n-1)\pi y}{b}\right) e^{i(\omega/U)x} \qquad (6)$$

In this case the propagation speed is equal to the velocity of the media. According to the usual jargon of acoustics and electromagnetics, the Fourier series terms represented by the cosine term in Eq. (6) are called modes. For example, for n equal to 1, the transverse shape (y-dimension) is plane and this is commonly called mode 1 or simply plane wave propagation. Mode 2 and higher are represented by the more complicated shapes defined by the cosine term and are called higher order mode propagation. In general, discontinuities of any kind, such as the metal blade in Fig. 3, will generate higher order modes because the uniform pattern is disturbed by the discontinuity.

BOUNDARY CONDITIONS

A variety of boundary conditions will be used in the finite element solution of Eq. (4). Each of these conditions will now be briefly discussed.

Input Conditions

The analysis assumes a given number N_m of positive going A^+_N waves. These waves (modes) effectively set the level of the scalar temperature field in the finite element region. In most of the example solutions to be presented, a plane wave input is assumed; that is, A^+_1 is taken as unity and the rest of the higher modal amplitudes are assumed zero.

Temperature Continuity

The temperature field is continuous across an interface except where heat sources are present. Thus,

$$\theta_a = \theta \quad (x = 0 \quad 0 \le y \le b) \qquad (7)$$

where θ_a is the modal representation of the temperature field in the analytical inlet region given by Eq. (A6) of Appendix A and θ represents the finite element approximation for temperature at the interface. The hat over θ implies an approximate finite element numerical solution to the true solution. Similar equations are used at the exit. For more details, see Baumeister 1986, Eqs. (43) to (52).

Heat Continuity

Heat flux continuity at the interface requires that

$$k_x \nabla\theta \cdot \bar{n} = -k_a \frac{\partial \theta_a}{\partial x} \qquad \text{(inlet)} \qquad (8)$$

$$k_x \nabla\theta \cdot \bar{n} = +k_b \frac{\partial \theta_b}{\partial x} \qquad \text{(exit)} \qquad (9)$$

The sign change in Eqs. (8) and (9) comes directly from the change of the unit outward normal.

Insulated Wall

At the insulated wall, the gradient of temperature will be zero normal to the boundary. Thus the last required boundary condition is

$$\nabla\theta \cdot \bar{n} = 0 \qquad (10)$$

FINITE ELEMENT THEORY

The finite element formulation of the energy equation was generated by using the weighted residual approach with the Galerkin approximation to obtain an integral form of the variable property wave equation over the whole global domain. The continuous domain is first divided into a number of discrete areas as shown in Fig. 3(b). This pattern as well as a symmetrical diamond pattern (Baumeister 1986, Fig. 9) were employed.

In the classical weighted residual manner, the temperature field is curve fitted in terms of all the unknown modal values $\theta(x_i,y_i)$. The finite element aspects of converting Eq. (4) and the boundary conditions into an appropriate set of global difference equations can be found in text books (Sergerlind, 1976) as well as Ref. 4 and for conciseness will not be presented herein.

ORIGINAL PAGE IS
OF POOR QUALITY

SIMPLIFIED ANALYSIS

In Appendix B, a simple theoretical model has been developed to predict the thermal transfer coefficient of a thermal disturbance in air (medium number 1) into a semi-infinite solid medium (medium number 2). The theory is shown by the solid line in Fig. 5. The simplified analysis will be useful in interpreting the more exact numerical results. The wall to gas temperature transfer function shown on the ordinate is a measure of the magnitude of temperature penetration into the solid. The key property group gamma developed in Appendix B indicates that the thermal transfer into the blade is proportional to

$$\Gamma = \frac{n}{k}\left(\frac{2\alpha}{\omega}\right)^{1/2} \qquad (11)$$

As seen in Eq. (11), the higher the heat transfer coefficient, the better the energy transfer or impedance match between the media. The transfer function ranges from zero (no penetration) to unity (full penetration) at the surface of the solid. The disturbance temperature will fall quickly in the solid material (see Eq. (A10)), thus giving rise to large thermal stresses.

Heat transfer coefficient on turbine blades are on the order of 1200 W/m^2 K (Simoneau, 1985, Fig. 10) to 5700 W/m^2 K in high pressure applications (Gladden and Proctor, 1985, Fig. 8). With a stainless steel blade experiencing a driving frequency of 500 Hz, the simple theory predicted a very low temperature transfer function as shown by the calculated values near gamma of 0.01 in Fig. 5. Consequently, thermal wave propagation in conventional gas turbine engines generally have very low thermal transfer coefficients and does not represent a problem.

Higher heat transfer coefficients, however, will lead to a better impedance match. In the SSME (Space Shuttle Main Engine) turbopump turbine, maximum heat transfer coefficients of 280 000 W/m^2 K have been predicted (Abdul-Aziz, 1987). Figure 5 displays transmission functions on the order of 20 percent in the stainless steel wall at a driving frequency of 1000 Hz.

Recent research (Metal Working News, 1987) at the NASA Lewis Research Center as well as industry has been concerned with ceramic coating of turbine blades to allow operations at higher gas temperature and achieve greater power plant efficiencies. In the schematic shown in Fig. 6, thermal barrier coatings (TBC) reduce the metallic blade temperature by adding a thin insulator to the outer surface. The low thermal conductivity of the ceramic effectively insulates the steady heat from penetrating the blade. However, as seen in Eq. (11), smaller values of the thermal conductivity k drives the value of gamma to larger values. A ceramic blade in the SSME environment had a transfer function of nearly 70 percent, as shown in Fig. 5.

RESULTS OF NUMERICAL ANALYSIS

The finite element theory will now be applied to some simple examples for code validation and to some typical hot gas turbine environments. The true value of the finite element theory would be in evaluating configurations with multiple ceramic and metallic layers or other geometrical complications.

Example 1 - Very Low Velocity Insulated Duct

Consider the problem of an infinitely long duct with insulated walls and with a single higher order mode ($n = 3$) propagating to the right from minus infinity. The amplitude of the wave is assumed unity at an axial position of x equals zero with a frequency of ω Hz. The ratio of Ub/α_x has a value of 50. For this case, the right going wave is moderately damped as shown in Figs. 7 and 8.

As seen in Fig. 7, the exact analytical results for the real and imaginary temperatures and the finite element analysis are in very good agreement. The real and imaginary solutions will generally display the spatial oscillating nature of the transformed time independent $\theta(x,y)$ solution. Figure 8 displays similar good agreement between the exact analytical and the finite element theories for the magnitude of the temperature oscillation. As seen in Fig. 8, the magnitude of the thermal wave decays because the thermal damping coefficient as predicted by the theory is large indicating that the waves energy is diffused into the fluid. The magnitude of θ_T is defined as

$$\left|\theta_T\right| = \left|\theta e^{i\omega t}\right| = \sqrt{\text{Real }(\theta)^2 + \text{Imag }(\theta)^2} \qquad (12)$$

As seen in Figs. 7 and 8, the variable time does not appear. At a particular location, the disturbance temperature θ_T rises and falls according to the harmonic forcing input conditions, defined by Eq. (2). Physically, the magnitude in Eq. (12) represents the peak value of the disturbance temperature at a given location at a particular time.

In addition to these checks, the velocity, mode number, and fluid properties (α_y) were altered to check the physical significants of all the terms in Eq. (A6) for further code validation. In all cases, the finite element and exact analysis were in agreement.

Example 2 - Insulated Turbine Duct

To model a typical turbojet turbine hot engine section, this example of the finite element technique considers the propagation of the a positive going plane thermal disturbance of 500 Hz in air moving at a Mach number of 0.5 in an insulated duct without an absorbing duct wall. In this and all the examples to follow, the fluid in the main channel is assumed to be air at 2060 °F. Symmetrical diamond triangles were used to discretize the duct. The amplitude of the wave is assumed unity at the axial position of x equal to zero. The plane nature of the impinging wave is indicated by the vertical line shown in the upper portion of Figs. 9 and 10, in contrast to the higher order mode shown in the upper portion of Fig. 7. Again, in this case the known analytical solution Eq. (A6) was in agreement with the numerical calculations. As seen in Fig. 10, at this high Mach number the magnitude of the thermal wave remains at constant amplitude because none of its energy is lost to the insulated wall and because the thermal damping coefficient displayed in Fig. 4 is near unity.

The finite element solutions in Figs. 9 and 10 in the region for $x/b = 0$ to 1 were determined from the nodal values of the grid points. However, there are no grid points in the region for x/b greater than 1, as shown by the upper schematic of Fig. 9. The finite element values designated by the symbols for x greater than 1 in the lower plot of Fig. 9 or Fig. 10 are reconstructed values from Eq. (A6) using the

transmitted mode amplitudes predicted by the finite element program. These are designated finite element solutions because the finite element analysis hasdetermined the generally unknown modal reflection A^-_n and transferred B^+_n coefficients. In this case, B replaces A in Eq. (A6) to represent the solution in the exit region. In the exit region, B^+_1 equals 1 and higher order B^+_n are nearly zero since only a plane wave exists. The B^-_n are zero since waves traveling in the negative direction at the exit have been assumed zero.

As seen in Fig. 9, for a frequency of 500 Hz, the wavelength associated with the phase nature of the thermal disturbance is on the order of the length of the finite element region which was chosen to model a typical turbine passage. Generally 12 elements per oscillation would be need for accurate calculations. For greater accuracy more elements were employed in this analysis than required.

Example 3 - STAINLESS STEEL DUCT WALL

Figure 11 shows a configuration with a stainless steel absorber region along the upper wall. Only a very thin wall was required since thermal disturbances can only penetrate a short distance into metallic surfaces. Since there is no flow in the metallic blade, the wave length of the spatial oscillation will be proportional to α/ω, as seen by the second term in Eq. (A10). For stainless steel, the size of the elements in the vertical direction was required to be a factor of 10 smaller than in the air duct, because of the very small wavelength in the metallic blade. The axial wave propagation in the blade itself is determined only in an approximate manner since the same grid spacing used in the main air duct was used in the metal blade.

Figure 11 displays contour plots of the magnitude of the temperature field in the stainless steel wall. The maximum temperature in the blade occurs at the tip of the blade at x/b equals 0.1 and y/b equals 1.0. As shown in Fig. 11, the maximum disturbance nondimensional wall temperature (max value of 1) is 0.00934 which is very small, and quantitatively agrees with the analytical predictions of Fig. 5. Consequently, thermal stress resulting from combustor generated thermal waves will not be a problem in a plug flow configuration.

Example 4 - Turbulent Flow Approximation

As discussed in the Simplified Analysis section, the high convective heat transfer coefficient associated with turbulent flow will produce a better energy transfer between the hot convective gases and the absorbing duct walls. An exact prediction of thermal disturbance propagation in turbulent flow would require coupling the continuity, momentum, and energy equations. For simplicity, the present analysis will now be empirically modified to roughly account for turbulent flow.

Using the even grid system of Fig. 3, the transverse thermal conductivity k_y in the two elements adjacent to the wall are now defined as

$$k_y = h\delta \qquad (13)$$

where h is the desired heat transfer coefficient and the gap δ represents the height of the elements. The heat transfer in the SSME (Space Shuttle Main Engine) will be used. In this case maximum heat transfer coefficients of 280 000 W/m^2 K is used with an assumed driving thermal wave frequency of 1000 Hz produced by temporal fuel burning oscillations similar to those shown in Fig. 2.

In addition, to simulate the convective mixing of the thermal energy by the turbulent flow in the central portion of the turbine duct, the ratio of conductivity in the y direction to the x direction was taken as 10 000. This assumption will alter the phase relationship in the higher order modes according to Eq. (A9) of Appendix A and introduces some reflections from the turbulent element.

Numerical results indicate the maximum transfer function of 0.2 or 20 percent of the maximum thermal wave temperature will enter the ceramic under the assumed conditions. This is less than the 70 percent predicted by the simple theory of Appendix B, which assumed a uniform bulk fluid temperature, as defined in Eq. (B12). However, as shown in Fig. 12, the finite element analysis predicts a decrease of the disturbance temperature field near the upper ceramic wall of the air duct, as shown by the disturbance temperature contour plots. The contour plot indicates a bulk temperature of approximately 30 percent of the entrance plane wave. If the uniform mean field temperature of the simple model were reduced by 30 percent, the simple analytical model results and the finite element results would be in close agreement. Considering the assumptions required to modify the plug flow theory to model turbulent flow, this agreement is reasonable.

CONCLUDING REMARKS

A finite element model was developed to solve for the disturbance temperature field in a duct with plug flow. The derivations from the governing equations assumed that the material properties could vary with position resulting in a nonhomogeneous variable property two-dimensional thermal wave equation. This eliminates the necessity of finding interface conditions between the different materials.

Validation examples showed excellent agreement between finite element and exact analytical solutions. Numerical examples indicated that thermal waves in conventional turbofan engines will not be a problem. However, thermal waves could possibly lead to significant thermal fatigue in high heat transfer regions such as in the SSME turbopump turbine, especially if thermal barrier coatings are used.

APPENDIX A - DISTURBANCE PROPAGATION

In the presence of uniform flow in a channel with insulted walls, the propagation of thermal disturbances is governed by the convected energy Eq. (3) in the body of this report. If the fluid properties are assumed constant, Eq. (3) can be rewritten as

$$\frac{\partial^2\theta}{\partial x^2} - \frac{U}{\alpha_x}\frac{\partial\theta}{\partial x} + \frac{\alpha_y}{\alpha_x}\frac{\partial^2\theta}{\partial y^2} - \frac{1}{\alpha_x}\dot{\theta} = 0 \qquad (A1)$$

where the thermal diffusivity α is defined as

$$\alpha = \frac{k}{\rho C} \qquad (A2)$$

Using separation of variables

$$\Theta = X(x)\,Y(y) \tag{A3}$$

yields

$$\frac{1}{X}\frac{\partial^2 X}{\partial x^2} - \frac{U}{\alpha_x}\frac{1}{X}\frac{\partial X}{\partial x} - \frac{i\omega}{\alpha_x} = \frac{1}{Y}\frac{\alpha_y}{\alpha_x}\frac{\partial^2 Y}{\partial y^2} = \lambda^2 \tag{A4}$$

and λ becomes the separation constant. For insulated upper and lower walls ($\partial\Theta/\partial y = 0$), the eigenfunction solution for Y becomes

$$Y = \cos\left(\frac{(n-1)\pi y}{b}\right) \qquad n=1,2,3,\ldots \tag{A5}$$

The solution for X follows the standard form (assume $\exp(mx)$) to yield

$$\Theta(x,y) = \sum_{n=1}^{N_m} A_n^+ \cos\left(\frac{(n-1)\pi y}{b}\right) e^{(U/2\alpha_x - a_n)x}\, e^{-id_n x} + \sum_{n=1}^{N_m} A_n^- \cos\left(\frac{(n-1)\pi y}{b}\right) e^{(U/2\alpha_x + a_n)x}\, e^{+id_n x} \tag{A6}$$

where

$$a_n = \left[\frac{1}{2}\left[\left(\frac{n^*\pi}{b}\right)^2 + \left(\frac{U}{2\alpha_x}\right)^2\right] + \frac{1}{2}\sqrt{\left[\left(\frac{n^*\pi}{b}\right)^2 + \left(\frac{U}{2\alpha_x}\right)^2\right]^2 + 4\left(\frac{\omega}{2\alpha_x}\right)^2}\right]^{1/2} \tag{A7}$$

$$d_n = \frac{1}{a_n}\frac{\omega}{2\alpha_x} \tag{A8}$$

$$n^* = (n-1)\sqrt{\frac{\alpha_y}{\alpha_x}} \tag{A9}$$

Here, in Eq. (A6), the A^+_n is the amplitude of the positive going waves while A^-_n is the amplitude of negative going waves.

No Flow

For no convective flow ($U = 0$) and plane wave propagation to the right ($n=1$), Eq. (A6) reduces to

$$\Theta = A_1^+ \exp\left[-\left(\frac{\omega}{2\alpha_x}\right)^{1/2} x\right] \exp\left[-i\left(\frac{\omega}{2\alpha_x}\right)^{1/2} x\right] \tag{A10}$$

This is the classic solution as commonly given in text books ((Arpaci, 1966), p. 329). In contrast to electromagnetic waves, thermal waves in a stationary medium are highly damped. For example, a thermal wave at a frequency of 500 Hz propagating in air at 2460 R ($\alpha = 2.76$ cm^2/sec) has a damping factor of 23.82/cm. Clearly, thermal waves at frequencies of 500 Hz or higher can not propagate in stationary air.

Large Mean Flow

For large values of the mean velocity U, Eq. (A6) can be approximated by

$$\Theta = A_n^+ \cos\left(\frac{(n-1)\pi y}{b}\right) e^{-i(\omega/U)x} \tag{A11}$$

Most important, the damping term has cancelled and thermal waves can propagate undamped in the duct like their analogous counter parts in acoustics and electromagnetics. As seen in Eq. (A11), the velocity of the thermal disturbance is equal to the velocity of the medium for all modes. This contrasts with acoustics, for example, for which each higher order mode has its own propagation speed.

The value of the attenuation constant in Eq. (A6) for a plane thermal wave at a frequency of 500 Hz in air is shown in Fig. 4. As seen in Fig. 4, for Mach numbers greater than 0.02 the attenuation factor approaches one (no attenuation).

APPENDIX B - IMPEDANCE MATCHING

The transmission of a thermal wave in a gaseous medium into a solid surface will be addressed in this section.

No Flow

When a thermal wave is incident on a material that has properties different from that of the medium in which the wave originated, part of the wave's energy is reflected and part is transmitted. This situation is similar to Acoustics and Electromagnetics. Consider the case of normal incidence of a plane wave in medium 1 contacting the medium 2 both of which are infinite in extent at coordinate x equal to zero. In region 1, the incident and reflected wave can be expressed as

$$\Theta = \Theta_0\, e^{-\beta_1 x} + \Theta_r\, e^{+\beta_1 x} \tag{B1}$$

where the complex propagation constant is equal to

$$\beta_1 = a_1 + id_1 \tag{B2}$$

from Eqs. (A7) and (A8) with U set to zero. In region 2, only a positive going wave exists, such that

$$\Theta = \Theta_t\, e^{-\beta_2 x} \tag{B3}$$

Assuming the magnitude of the incident wave is given, the object of this section is to find the magnitude of the reflected Θ_r and transmitted Θ_t waves as a function of the thermal properties of the media.

Continuity of the temperature at the interface between the two medium requires that

$$\Theta_0 + \Theta_r = \Theta_t \tag{B4}$$

In addition, the heat balance at the interface requires that

$$-k_1 \left.\frac{\partial\Theta}{\partial x}\right|_{x=0} = -k_2 \left.\frac{\partial\Theta}{\partial x}\right|_{x=0} \tag{B5}$$

or

$$k_1(-\beta_1\Theta_0 + b_1\Theta_r) = k_2(-\beta_2\Theta_t) \tag{B6}$$

Solving Eq. (B4) and B(6) simultaneously for Θ_r and Θ_t yields

$$\frac{\theta_r}{\theta_o} = \left(\frac{n_1 - n_2}{n_1 + n_2}\right) \tag{B7}$$

$$\frac{\theta_t}{\theta_o} = \frac{2n_1}{n_1 + n_2} \tag{B8}$$

where the thermal impedance n is defined as

$$n_1 = k_1\beta_1 = -i\,\frac{(1+i)}{\sqrt{2}}\sqrt{\frac{\omega}{\alpha_1}} \tag{B9}$$

The value of β in the absence of flow is found from Eqs. (B2), (A6) and (A7).

For no reflections, n_1 equals n_2.

$$k_1\rho_1 c_1 = k_2\rho_2 c_2 \tag{B10}$$

which is independent of the driving frequency.

For an air to metallic surface (stainless steel)

$$\frac{\theta_t}{\theta_o} = 0.001 \tag{B11}$$

Clearly, thermal waves at any frequency in stationary air can not effectively penetrate a metallic surface.

Convective Flow

In contrast to the no flow example, consider medium 1 to be at a uniform mean temperature θ_o such that

$$\theta = \theta_o\, e^{i\omega t} \tag{B12}$$

and in medium 2

$$\theta = \theta_t e^{-\beta_2 x} e^{i\omega t} \tag{B13}$$

where β_2 is defined by Eq. (B2).

Neglecting reflection, a simple instantaneous heat balance at the interface x equal to zero requires that

$$h_1(\theta_o - \theta_t) = -k_2 \frac{\partial\theta}{\partial x}\bigg|_{x=0} = +k_2\beta_2\theta_t \tag{B14}$$

Solving for θ_t yields

$$\frac{\theta_t}{\theta_o} = \frac{1}{1 + k_2\frac{\beta_2}{h_1}} = \frac{1}{1 + \frac{k_2}{h_1}(1+i)\left(\frac{\omega}{2\alpha_2}\right)^{1/2}} \tag{B15}$$

Solving for the real part of this ratio yields

$$\left|\text{Real}\left(\frac{\theta_t}{\theta_o}\, e^{i\omega t}\right)\right| = \frac{\Gamma}{\sqrt{\Gamma^2 + 2\Gamma + 2}} \tag{B16}$$

where

$$\Gamma = \frac{h_1}{k_2}\left(\frac{2\alpha_2}{\omega}\right)^{1/2} \tag{B17}$$

For small values of Γ, Eq. (B16) can be approximated as

$$\text{Real}\left(\frac{\theta_T\, e^{i\omega t}}{\theta}\right) \approx \frac{\Gamma}{1.41} = \frac{h_1}{\sqrt{k_2\rho_2 c_2 \omega}} \tag{B18}$$

Thus, for large energy transfer the heat transfer coefficient should be large. Also, decrease in frequency, thermal conductivity, density or specific heat will improve the energy transfer.

REFERENCES

1. Abdul-Azis, A., Tong, M., and Kaufman, A., "Thermal Finite-Element Analysis of an SSME Turbine Blade," Paper presented at the 24th ASME/AIChE National Heat Transfer Conference, Pittsburgh, PA, Aug. 1987.

2. Arpaci, V.S., 1966, Conducting Heat Transfer, Addison-Wesley, Reading, MA.

3. Baumeister, K.J., 1986a, "Finite Element Analysis of Electromagnetic Propagation in an Absorbing Wave Guide," NASA TM-88866.

4. Baumeister, K.J., 1986b, "Effect of Triangular Element Orientation on Finite Element Solutions of the Helmholtz Equation," ASME Paper 86-WA/NSC-12. (NASA TM-87351).

5. Bird, R.B., Stewart, W.E., and Lightfoot, E.N., 1960, Transport Phenomena, John Wiley and Sons, New York.

6. Gladden, H.J., and Proctor, M.P., 1985, "Transient Technique for Measuring Heat Transfer Coefficients on Stator Airfoils in a Jet Engine Environment," AIAA Paper 85-1471. (NASA TM-87005).

7. Metalworking News, Vol. 14, No. 649, Monday, Sept. 21, 1987.

8. Norgren, C.T., and Riddlebaugh, S.M., 1985, "Advanced Liner-Cooling Techniques for Gas Turbine Combustors," AIAA Paper 85-1290. (NASA TM-86952).

9. Sergerlind, L.J., 1976, Applied Finite Element Analysis, John Wiley and Sons, New York.

10. Simoneau, R.J., 1985, "Heat Transfer in Aeropropulsion Systems," NASA TM-87066.

11. Sofrin, T.G., and Riloff, N., Jr., 1976, "Experimental Clean Combustor Program-Noise Study," NASA CR-135106.

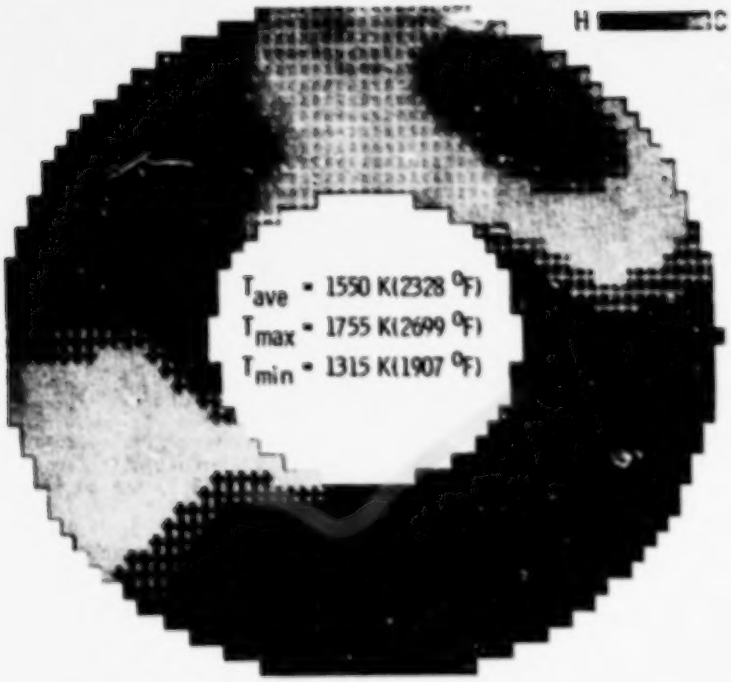

FIGURE 1. - TYPICAL COMBUSTOR OUTLET TEMPERATURE DISTRIBUTION (NORGREN, 1985).

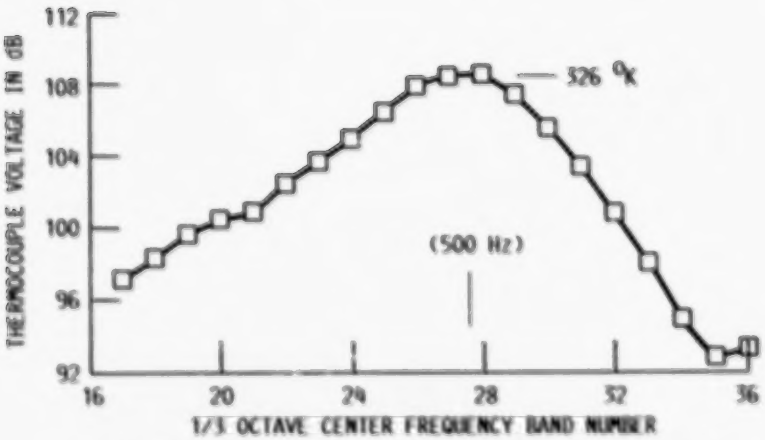

FIGURE 2. - COMBUSTOR GAS TEMPERATURE FLUCTUATIONS. RELATIVE SPECTRUM FOR H-6 COMBUSTOR AT IDLE (SOFRIN AND RILOFF, 1976) PEAK RMS TEMPERATURE EQUALS 326 °K.

ORIGINAL PAGE IS
OF POOR QUALITY

(a) GEOMETRICAL TURBINE BLADE PASSAGE SIMPLIFICATION.

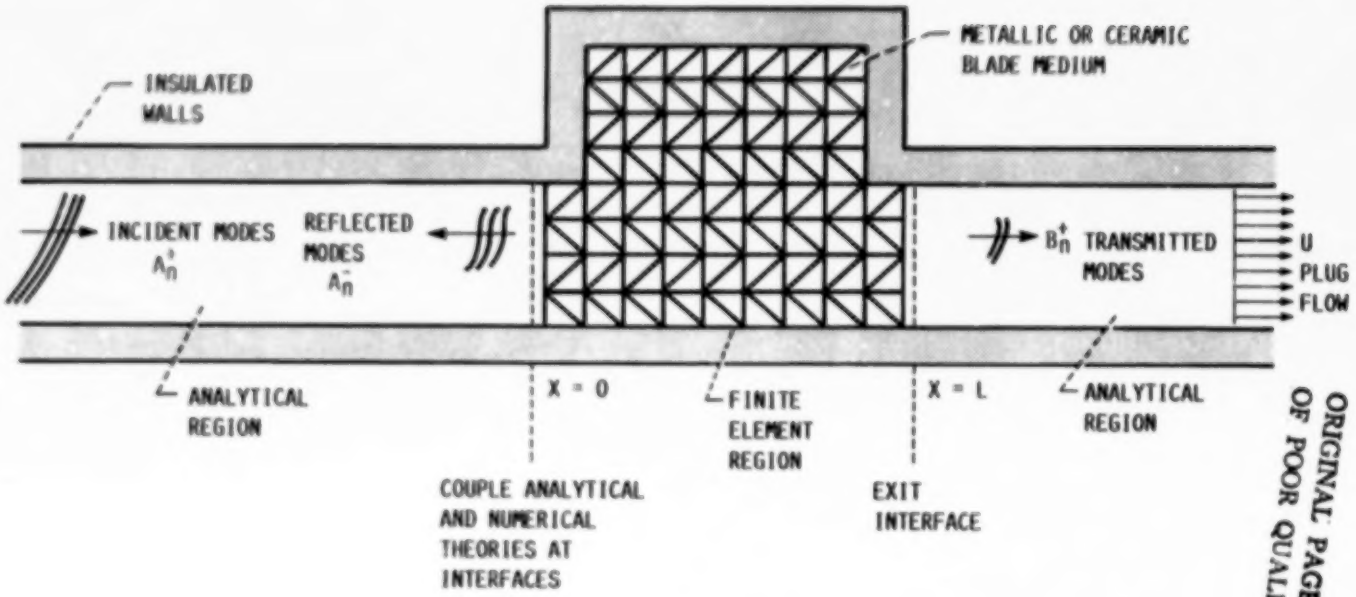

(b) FINITE ELEMENT STRUCTURE IN PASSAGE.

FIGURE 3. - TWO DIMENSIONAL DUCT FINITE ELEMENT MODEL.

ORIGINAL PAGE IS OF POOR QUALITY

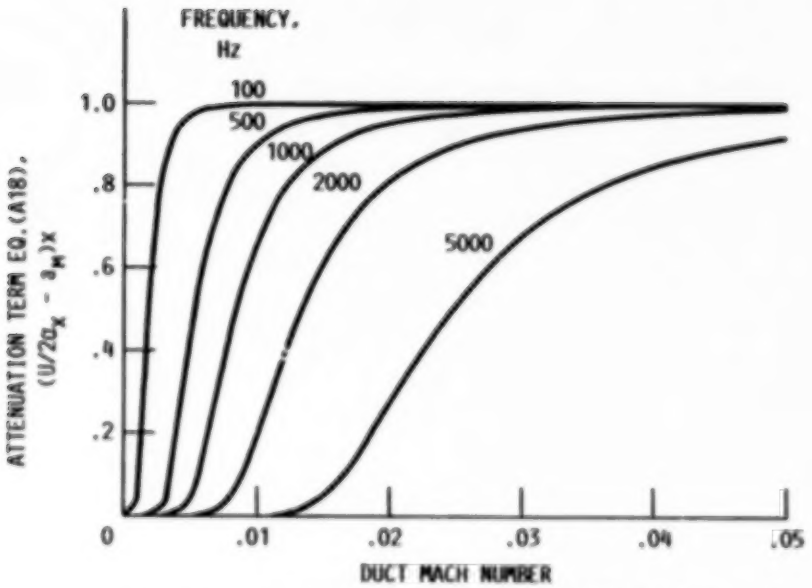

FIGURE 4. - EFFECTIVE ATTENUATION TERM FOR A PLANE WAVE IN AIR AT 3500 R FOR A DUCT 2.54 cm HIGH AT x = 2.54 cm.

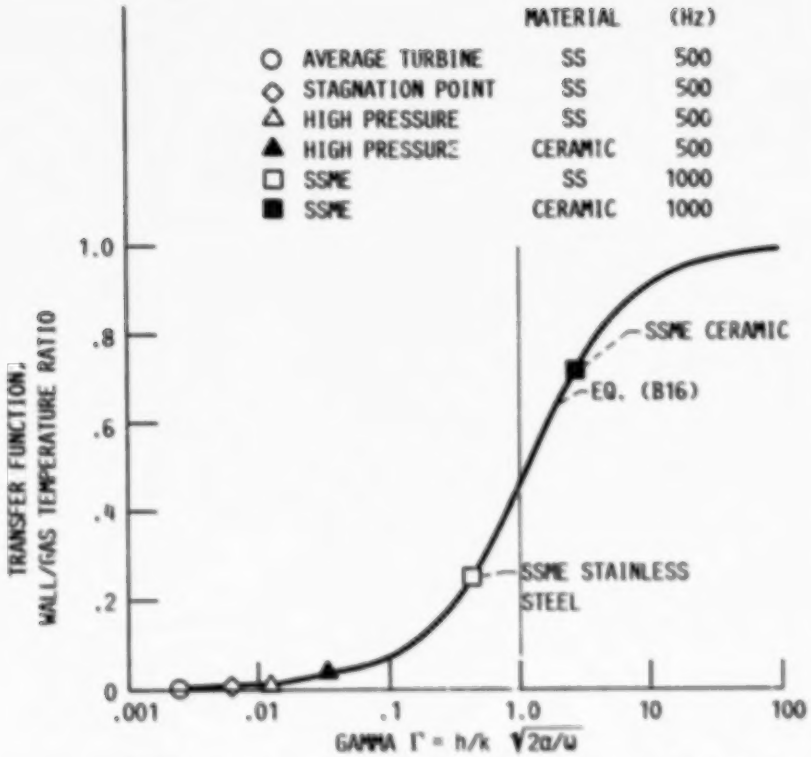

FIGURE 5. - MAGNITUDE OF THE THERMAL TRANSFER FUNCTION FOR VARIOUS HEAT TRANSFER COEFFICIENTS. STAINLESS STEEL AND CERAMIC BLADES.

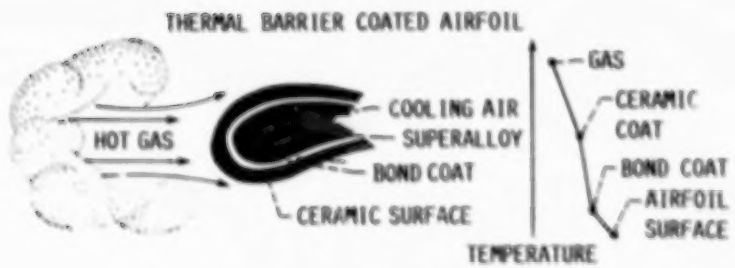

FIGURE 6. - HOW THERMAL BARRIER COATINGS FUNCTION (REF. METALWORKING NEWS, 1987).

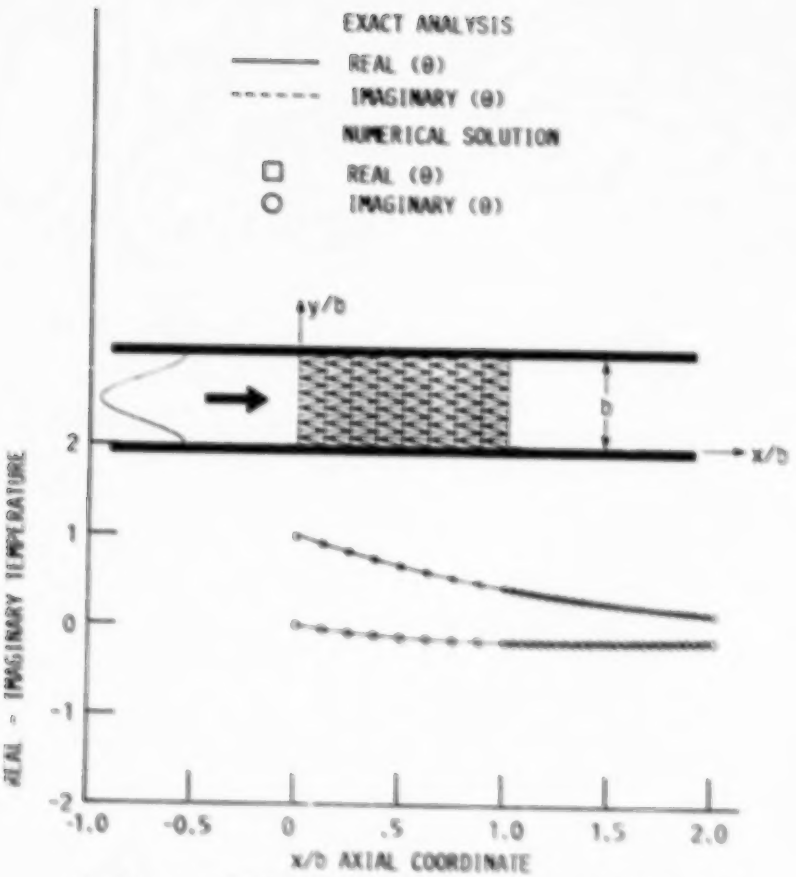

FIGURE 7. - COMPARISON OF REAL AND IMAGINARY TEMPERATURE VARIATION ALONG THE LOWER WALL (y/b = 0) IN A UNIFORM DUCT WITH INSULATED WALLS AS OBTAINED BY USING AN EXACT SOLUTION AND A FINITE ELEMENT SOLUTION FOR A MODE 3 INCIDENT AT x/b = 0. WITH FREQUENCY OF π Hz AND Ub/α EQUAL TO 50.

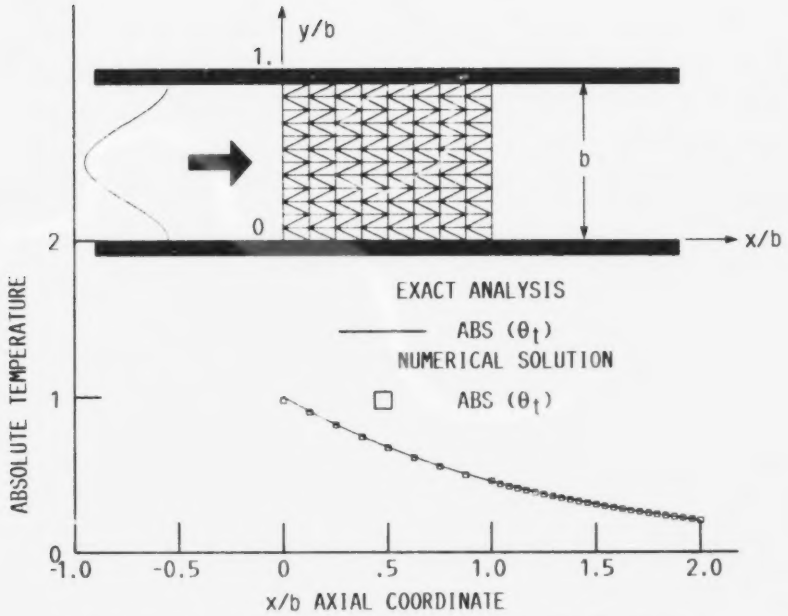

FIGURE 8. - COMPARISON OF MAGNITUDE OF TEMPERATURE VARIATION ALONG THE LOWER WALL (y/b = 0) IN A UNIFORM DUCT WITH INSULATED WALLS AS OBTAINED BY USING AN EXACT SOLUTION AND A FINITE ELEMENT SOLUTION FOR A MODE 3 INCIDENT AT x/b = 0. WITH FREQUENCY OF π Hz AND Ub/α = TO 50.

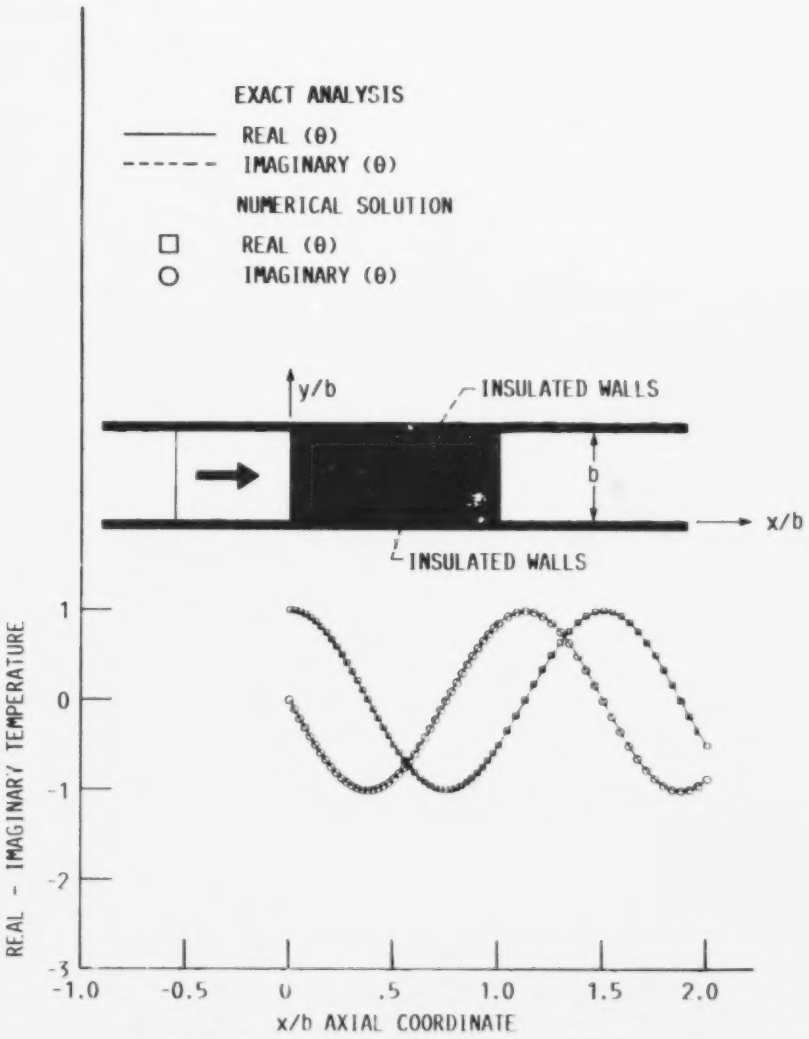

FIGURE 9. - COMPARISON OF TEMPERATURE VARIATION ALONG LOWER WALL WITH AIR FLOWING AT MACH 0.5 IN A UNIFORM DUCT WITH INSULATED WALLS AS OBTAINED BY USING AN EXACT SOLUTION AND A FINITE ELEMENT SOLUTION FOR A PLANE WAVE (MODE) INCIDENT AT x = 0 WITH f = 500.0 Hz, AND N_M = 3.

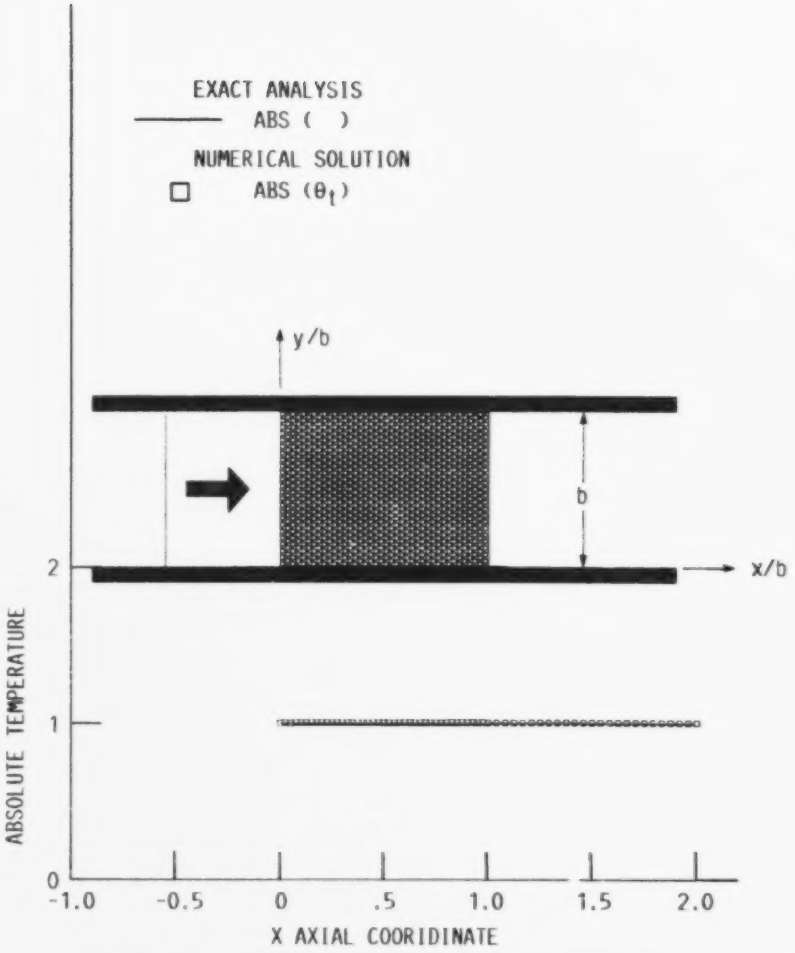

FIGURE 10. - COMPARISON OF MAGNITUDE OF TEMPERATURE VARIATION ALONG LOWER WALL WITH AIR FLOWING AT MACH 0.5 IN A UNIFORM DUCT WITH INSULATED WALLS AS OBTAINED BY USING AN EXACT SOLUTION AND A FINITE ELEMENT SOLUTION FOR A PLANE WAVE (MODE 1) INCIDENT AT x = 0 WITH f = 500.0 Hz, AND N_M = 3.

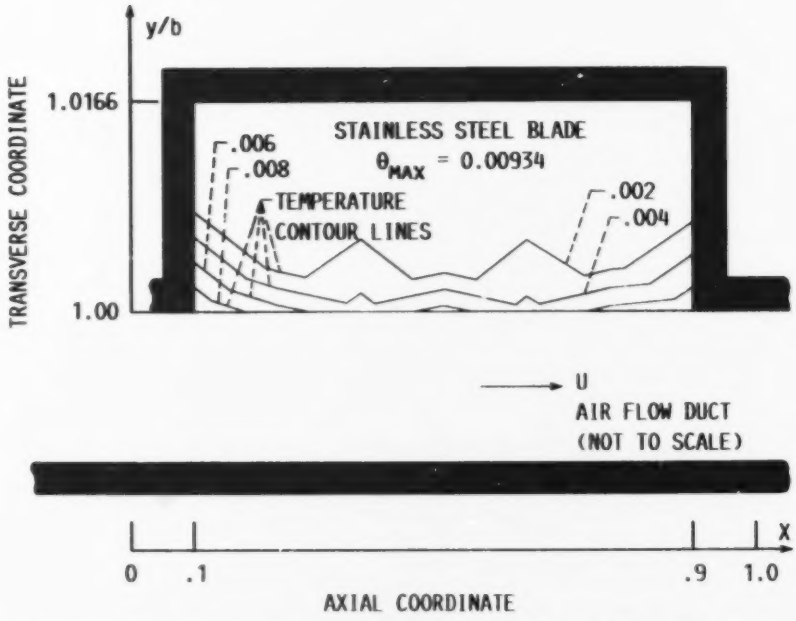

FIGURE 11. - MAGNITUDE OF THE TEMPERATURE FIELD CONTOURS IN THE BLADE WALL MATERIAL ABOVE THE AIR DUCT WITH UNIFORM PLUG FLOW IN DUCT.

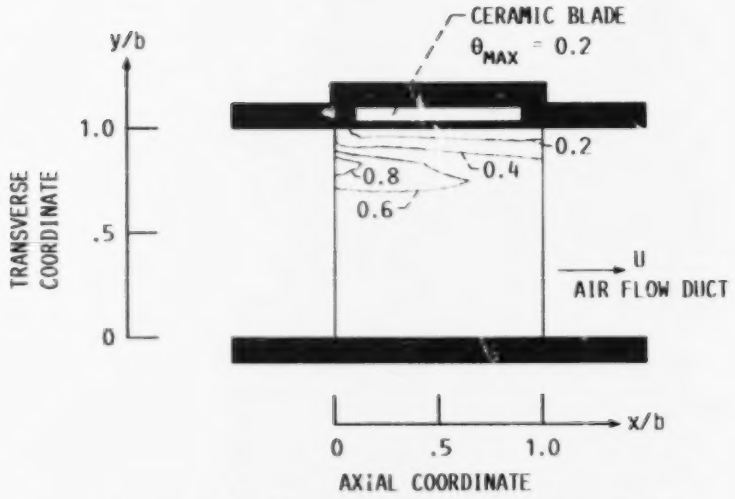

FIGURE 12. - MAGNITUDE OF THE TEMPERATURE FIELD CONTOURS IN THE AIR DUCT WITH EMPIRICAL MODIFICATION IN THE FLOW FIELD TO ACCOUNT FOR TURBULENT HEAT TRANSFER.

NASA
National Aeronautics and Space Administration

Report Documentation Page

1. Report No.	2. Government Accession No.	3. Recipient's Catalog No.
NASA TM-100815		

4. Title and Subtitle	5. Report Date
Unsteady Heat Transfer in Turbine Blade Ducts: Focus on Combustor Sources	6. Performing Organization Code

7. Author(s)	8. Performing Organization Report No.
Kenneth J. Baumeister and Ronald Huff	E-4000
	10. Work Unit No. 505-62-21

9. Performing Organization Name and Address	11. Contract or Grant No.
National Aeronautics and Space Administration Lewis Research Center Cleveland, Ohio 44135-3191	13. Type of Report and Period Covered: Technical Memorandum

12. Sponsoring Agency Name and Address	14. Sponsoring Agency Code
National Aeronautics and Space Administration Washington, D.C. 20546-0001	

15. Supplementary Notes

Prepared for the National Heat Transfer Conference sponsored by the American Society of Mechanical Engineers, Houston, Texas, July 24-27, 1988. Kenneth J. Baumeister, NASA Lewis Research Center; Ronald Huff, Huff and Associates, Cleveland, Ohio.

16. Abstract

Thermal waves generated by either turbine rotor blades cutting through nonuniform combustor temperature fields or unsteady burning could lead to thermal fatigue cracking in the blades. To determine the magnitude of the thermal oscillation in blades with complex shapes and material compositions, a finite element Galerkin formulation has been developed to study combustor generated thermal wave propagation in a model two-dimensional duct with a uniform plug flow profile. The reflection and transmission of the thermal waves at the entrance and exit boundaries are determined by coupling the finite element solutions at the entrance and exit to the eigenfunctions of an infinitely long adiabatic duct. Example solutions are presented for a variety of cases. In general, thermal wave propagation from an air passage into a metallic blade wall is small and not a problem. However, if a thermal barrier coating is applied to a metallic surface under conditions of high heat transfer, a good impedance match is obtained and a significant portion of the thermal wave can pass into the blade material.

17. Key Words (Suggested by Author(s))	18. Distribution Statement
Finite element; Unsteady; Harmonic Heat transfer	Unclassified - Unlimited Subject Category 34

19. Security Classif. (of this report)	20. Security Classif. (of this page)	21. No of pages	22. Price*
Unclassified	Unclassified	18	A02

NASA FORM 1626 OCT 86

*For sale by the National Technical Information Service, Springfield, Virginia 22161